RESEARCH ARTICLE | JUNE 27 2017

High-temperature thermocline TES combining sensible and latent heat - CFD modeling and experimental validation FREE

Simone A. Zavattoni; Lukas Geissbühler; Maurizio C. Barbato; Giw Zanganeh; Andreas Haselbacher; Aldo Steinfeld

AIP Conf. Proc. 1850, 080028 (2017)
https://doi.org/10.1063/1.4984449

High-Temperature Thermocline TES Combining Sensible and Latent Heat - CFD Modeling and Experimental Validation

Simone A. Zavattoni[1], Lukas Geissbühler[2], Maurizio C. Barbato[1, a)], Giw Zanganeh[3], Andreas Haselbacher[2], Aldo Steinfeld[2]

[1] *Department of Innovative Technologies, SUPSI, 6928 Manno, Switzerland*
[2] *Department of Mechanical and Process Engineering, ETH Zurich, 8092 Zurich, Switzerland*
[3] *Airlight Energy Manufacturing SA, 6710 Biasca, Switzerland*

[a)] Corresponding author: maurizio.barbato@supsi.ch

Abstract. The concept of combined sensible/latent heat thermal energy storage (TES) has been exploited to mitigate an intrinsic thermocline TES systems drawback of heat transfer fluid outflow temperature reduction during discharging. In this study, the combined sensible/latent TES prototype under investigation is constituted by a packed bed of rocks and a small amount of encapsulated phase change material ($AlSi_{12}$) as sensible heat and latent heat sections respectively. The thermo-fluid dynamics behavior of the combined TES prototype was analyzed by means of a computational fluid dynamics approach. Due to the small value of the characteristic vessel-to-particles diameter ratio, the effect of radial void-fraction variation, also known as channeling, was accounted for. Both the sensible and the latent heat sections of the storage were modeled as porous media under the assumption of local thermal non-equilibrium (LTNE). The commercial code ANSYS Fluent 15.0 was used to solve the model's constitutive conservation and transport equations obtaining a fairly good agreement with reference experimental measurements.

INTRODUCTION

Year by year, the topic of large-scale thermal energy storage (TES) systems for high-temperature applications such as concentrating solar power (CSP) or adiabatic compressed-air energy storage (A-CAES), is receiving increased attention from R&D public and private institutions with the major aims of technical improvements and cost reduction. In CSP especially, TES is being recognized as key component for maintaining competitiveness, against solar photovoltaics, enabling solar energy to be dispatchable. At the end of 2015 the global CSP operating capacity reached about 4.8 GW with an increment of 420 MW with respect to 2014. Furthermore, for the first time, all the CSP plant built in 2015 are equipped with a TES system [1]. Remarkable examples are: (a) the 110 MW Crescent Dunes facility (US) with 10 h storage capacity and (b) the planned 200 MW Noor 2 facility (Morocco), currently under construction, with 7 h storage capacity [1].

The TES solution commonly exploited in commercial CSP plant is based on sensible heat storage, with oil or molten salts as storage media, in a two-tank configuration. Nevertheless, thermocline TES with a packed bed of low cost filler material can be considered as reliable, affordable, and efficient alternative solution for storing thermal energy. However, an intrinsic drawback of this solution is the decrease of the heat transfer fluid (HTF) outflow temperature, towards the end of discharging leading to a non-optimal working condition of the power block. This drawback can be mitigated if a TES based on latent heat would be exploited instead. However, the high cost of the phase change material (PCM) is among the limiting factors on its integration into a CSP plant. For this reason, the idea of adding a small amount of PCM on top of a packed bed was proposed, and experimentally investigated [2], with the aim of stabilizing the HTF outflow temperature during discharging.

SolarPACES 2016
AIP Conf. Proc. 1850, 080028-1–080028-8; doi: 10.1063/1.4984449
Published by AIP Publishing. 978-0-7354-1522-5/$30.00

The present study aims at developing a 2D computational fluid dynamics (CFD) model to replicate the behavior of a combined sensible/latent heat storage which uses air as HTF. Furthermore, a lab-scale combined TES prototype was exploited to assess the accuracy of the numerical model by comparing the CFD simulation results with experimental data.

EXPERIMENTAL COMBINED SENSIBLE/LATENT HEAT STORAGE

The lab-scale combined TES prototype under investigation is depicted in Fig. 1. A packed bed of gravel, consisting of different rocks types such as limestone, quartzite, sandstone and gabbro, was exploited as sensible heat section of the TES. The average particles diameter and void-fraction were 32 mm and 0.4 respectively; the total packed bed mass was 245 kg. Concerning the latent heat section of the TES, because of its melting temperature range (573-577 °C) suitable for CSP applications, high heat of fusion (466 kJ/kg) and high thermal conductivity (160 W/m·K), $AlSi_{12}$ alloy was selected as proper PCM material [2]. The latter was encapsulated in AISI 316 steel tubes, 16 mm internal diameter and 1 mm thickness. The encapsulated PCM was positioned on top of the packed bed and distributed on four layers, constituted by 17 tubes each and oriented with an angle of 45°, forming a sort of tube bundle with an average void-fraction of 0.55. The total mass of the latent heat section of the TES was about 22.5 kg divided in 9.3 kg and 13.2 kg of PCM and encapsulation mass respectively.

Pebbles and encapsulated PCM were located into a 1.68 m high cylindrical AISI 304 stainless steel tank, 0.4 m external diameter and 3 mm thickness, leading to a total height of 1.27 m and 0.09 m for the former and the latter respectively. Because of the high-temperature, the upper part of the TES prototype was well insulated by means of a sandwich of different insulating materials such as Microtherm®, felt and rockwool, 20 mm, 40 mm and 100 mm thickness respectively. On the intermediate region of the TES prototype the insulation was constituted by felt and rockwool, 60 mm and 100 mm thickness respectively; while, on the lower part, only felt, 50 mm thickness, was exploited.

The configuration of the combined TES prototype is an open circuit in which air was the reference HTF. During charging, high-temperature air, up to 595°C, was fed through the TES from top where a metallic perforated plate is exploited to obtain an homogeneous distribution of the airflow over the entire cross-section. The HTF then delivers its thermal energy to the TES flowing through both the encapsulated PCM and the packed bed of gravel before leaving the TES from the bottom. Conversely, during discharging, the air flow was reversed and air at ambient temperature was fed through the prototype from the bottom. Another metallic perforated plate, 20 mm thickness, was exploited with the twofold aim of sustaining the packed bed own weight and homogenizing the air flow.

As depicted in the r.h.s. of Fig. 1, the prototype is equipped with several K-type thermocouples (TCs), along with a mass flow meter, to monitor the temperature and the HTF mass flow rate evolution during tests. The total capacity of the combined TES prototype is 42.3 kWh_{th}.

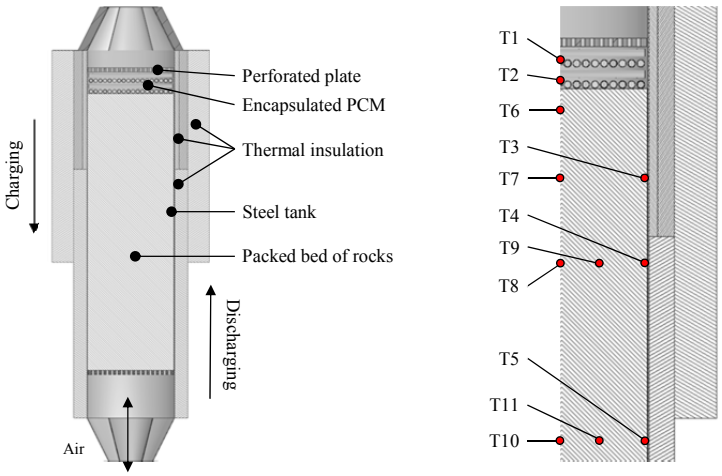

FIGURE 1. Schematic of the pilot-scale combined TES (l.h.s.) and TCs position (r.h.s.).

2D CFD MODEL

A transient CFD analysis was performed with the aim of evaluating the thermo-fluid dynamics behavior of the combined TES prototype. The axisymmetric characteristic of the prototype was exploited to build a 2D computational domain. Grid-independent results were obtained with a grid of about 360'000 quadrilateral cells. Mass, momentum, energy, turbulent kinetic energy and turbulent dissipation rate transport equations were numerically solved with the finite volume method (FVM) approach [3] by means of Fluent 15.0 code from ANSYS. Turbulence effects were accounted for by means of the realizable k -ε model [4] with enhanced wall treatment, as near-wall modeling method [5].

During the reference experimental test, a slight variation of the HTF inlet temperature and mass flow rate was observed before achieving constant values; therefore, to accurately replicate the experimental test, the measured variation of HTF temperature and mass flow rate was accounted for. Thermal energy losses, by means of convection and radiation, were also considered assuming an ambient temperature of 20°C and an external convective heat transfer coefficient of 5 W/(m^2·K). At the beginning of the time-dependent CFD simulation, namely at time t = 0 s, the combined TES prototype was assumed to be in thermal equilibrium with the environment with a dead-state temperature of 20°C.

The packed bed of pebbles and the bank of tubes were modeled exploiting the porous media approach [6]. With this strategy, the porous medium is characterized by means of four main parameters namely: the effective thermal conductivity (ETC), the void-fraction distribution, the permeability K and inertial resistance coefficient C2 (both related to the pressure drop evaluation). Due to the relatively high HTF flow velocity, in order to have a more accurate description of the heat transfer, local thermal non-equilibrium (LTNE model) between the solid matrix and the fluid phase was assumed; therefore, two separate conservation equations of energy (eq. 1 and eq. 2) are solved to model the heat transfer through the porous medium. The general conservation equation for energy solved for the fluid zone is [7]:

$$\begin{aligned}&\frac{\partial}{\partial_t}\left(\varepsilon\cdot\rho_f\cdot E_f\right)+\nabla\left(\vec{v}\cdot\left(\rho_f\cdot E_f+p\right)\right)=\\&=\nabla\left(\varepsilon\cdot k_f\cdot\nabla T_f-\left(\sum_i h_i\cdot J_i\right)+\left(\bar{\bar{\tau}}\cdot\vec{v}\right)\right)+S_f^h+h_{fs}\cdot A_{fs}\cdot\left(T_f-T_s\right)\end{aligned}\tag{1}$$

While, the general conservation equation for energy solved for the fluid zone is [7]:

$$\frac{\partial}{\partial_t}\left(\left(1-\varepsilon\right)\cdot\rho_s\cdot E_s\right)=\nabla\left(\left(1-\varepsilon\right)\cdot k_{s,eff}\cdot\nabla T_s\right)+S_s^h+h_{fs}\cdot A_{fs}\cdot\left(T_s-T_f\right)\tag{2}$$

The first three terms on the r.h.s. of eq.(1) represent energy transfer due to conduction, species diffusion, and viscous dissipation in the fluid phase respectively. The first term on the r.h.s. of eq.(2), diffusive term, represents the energy transfer due to conduction in the solid phase characterized by an effective thermal conductivity accounting for all the non-convective heat transfer mechanisms occurring into the packed bed. The remaining terms in the r.h.s. of eq.(1) and eq.(2) are volumetric source terms: the second to last represent a volumetric source terms arbitrary defined for the fluid and/or the solid phase respectively; while, the last terms represent the source terms due to non-equilibrium thermal model wherein h_{fs} and A_{fs} are the solid-to-fluid heat transfer coefficient and the interfacial area density, i.e. the ratio of the area of the fluid/solid interface and the volume of the packed bed, required to couple the two energy equations. A detailed description of the models implemented to evaluate the two coefficients can be found in the next sections. Air was assumed as incompressible ideal gas with thermo-physical properties assigned as piecewise linear interpolations of tabulated data [8].

All the model equations were solved with second order accurate numerical schemes [3]. The pressure-implicit with splitting of operators (PISO) algorithm and the pressure staggering option (PRESTO!) scheme were used to couple the velocity and pressure fields and to solve the pressure-correction equation. Convergence was considered achieved when mass, momentum and turbulence residuals were below 10^{-5} and energy residual was below 10^{-8}.

Sensible Heat Section

Void-fraction Distribution in a Generic Packed Bed of Non-spherical Particles

The void-fraction of a generic homogeneous packed bed, defined as the ratio of the void volume with respect to the total bed volume, depends mainly on particles arrangement. In the case of randomly packed equally sized spherical particles, the reference porosity in the bulk region ranges between 0.36 and 0.42 [9]. Near the containing wall, the arrangement of the particles is sensibly modified affecting the overall packing structure for a distance of approximately 5 d_p from the wall. In this near-wall region, the void-fraction distribution undergoes a sharp damped oscillatory variation, from a value close to unity at the wall down to a minimum of 0.2 at a distance of 0.5 d_p from the wall. Beyond the distance of about 5 d_p from the wall, the void-fraction approaches the value of the bulk region. The resulting reduced void-fraction leads to the development of a preferential flow in the near-wall region [10], i.e. uneven HTF mass flow rate distribution on the cross-section of the packed bed. This so-called wall effect, or channeling, can also be observed in packed beds of relatively rough non-spherical and not exactly equally sized particles, with the difference that the oscillatory behaviour is replaced by an exponential decay of the void fraction approaching the value of the bulk region after a rather short distance [11]. The average void-fraction in the packed bed is also affected as long as the vessel-to-particle diameter ratio is lower than 25-30 [10, 12]. The TES prototype under investigation is characterized by a vessel-to-particle diameter ratio of about 12.5; therefore, neglecting the effect of channelling can sensibly limit the accuracy of the model in predicting the heat and mass transfer into the packed bed due to macroscopic flow maldistribution. Because of that, a radial void-fraction distribution was implemented into the CFD model on the basis of the exponential decay function proposed by Hunt and Tien [13] and adapted for cylindrical vessels:

$$\varepsilon(r) = \varepsilon_{bulk} \cdot \left(1 + C \cdot exp\left(-N \cdot \frac{R-r}{d_p} \right) \right) \tag{3}$$

with the values of the constants C of 1.7 [14] or 1.36 [11] and N of 2 [15], 5 [11] or 6 [13]. In the present study, the values of 1.2 and 2 of C and N respectively were found to have a close approximation with experimental data.

Effective Thermal Conductivity and Heat Transfer in Packed Beds

According to the theoretical and experimental studies of Yagi and Kunii [16] and Kunii and Smith [17], the heat transfer mechanisms in packed beds of unconsolidated particles can be considered as the sum of two contributions: the heat transfer mechanisms independent on the fluid flow and those dependent on the lateral mixing of the fluid. In the case of packed bed with stagnant fluid (quiescent bed) five different heat transfer mechanisms take place: (1) thermal conduction through solid, thermal conduction (2) through the contact surfaces of two packings and (3) through the fluid film near the contact surface of two packings, radiant heat transfer (4) between surfaces of two packings and (5) between neighboring voids. The latter two have to be intended in the case the fluid is a gas. The remaining heat transfer mechanisms, occurring when fluid flows through the packed bed, are: (6) heat transfer by convection solid-fluid-solid and (7) heat transfer by advective mixing. On the basis of heat transfer mechanisms (1) to (5), the authors derived a model for predicting the stagnant ETC of the packed bed, made by homogeneous spheres, that reads [17]:

$$k_{ETC}^{0} = k_g \cdot \left[\varepsilon \cdot \left(1 + \frac{\beta \cdot h_{rv} \cdot d_p}{k_g} \right) + \frac{\beta \cdot (1-\varepsilon)}{\left(\frac{1}{\varphi} + \frac{d_p \cdot h_{rs}}{k_g} \right)^{-1} + \frac{2 \cdot k_g}{3 \cdot k_s}} \right] \tag{4}$$

The geometric factor β is related to the particles arrangement: in the case of close packing of spheres it assumes the value of 0.895; conversely, for the most loose packing its value should be unity. Therefore, for almost all actual

packed beds, β ranges between 0.9 and 1. The radiation heat transfer coefficients h_{rv} and h_{rs}, for the void-to-void and the solid surface to solid surface exchange respectively, are defined as follows [16]:

$$h_{rv} = 0.227 \cdot \left(1 + \frac{\varepsilon \cdot (1-\psi)}{2 \cdot \psi \cdot (1-\varepsilon)}\right)^{-1} \cdot \left(\frac{T}{100}\right)^3 \tag{5}$$

$$h_{rs} = \frac{0.227 \cdot \psi}{2-\psi} \cdot \left(\frac{T}{100}\right)^3 \tag{6}$$

For the range of the packed bed void-fraction between 0.26 and 0.476, the φ parameter can be computed as follows:

$$\varphi = \varphi_2 + (\varphi_1 - \varphi_2) \cdot \frac{\varepsilon - 0.26}{0.216} \tag{7}$$

In the field of numerical modeling, stagnant ETC is commonly exploited to model heat transfer in porous media since it allows to group all the non-convective heat transfer mechanisms within a single equivalent value. The remaining heat transfer mechanisms dependent on the fluid flow are accounted for by the numerical solution of the Navier-Stokes and energy transport equations. Therefore, the model derived by Kunii and Smith [17] was implemented in the CFD simulation, by means of purpose-built user-defined function, i.e. a "C" routine properly written to be linked to the solver, to accurately describe the heat transfer into the packed bed of the combined TES system under investigation.

Additional Details

The temperature variation of the thermo-physical properties of the rocks were extrapolated from lab-tests on different samples and implemented in the numerical model [18]. Temperature dependent properties of the insulating materials, obtained from the suppliers' datasheet, were also implemented.

The solid-to-fluid heat transfer coefficient, eq.(1) and eq.(2), was derived from the following empirical relation [19]:

$$Nu_{packed-bed} = \frac{h_{fs} \cdot d_p}{k_g} = \frac{2.06}{\varepsilon} \cdot Re_p^{0.425} \cdot Pr^{1/3} \tag{8}$$

valid for $90 \leq Re_p \leq 4'000$ and $Pr \approx 0.7$. The Reynolds number is defined in terms of particle diameter and superficial velocity V_s that would exist assuming an empty channel:

$$Re_p = \frac{\rho \cdot V_s \cdot d_p}{\mu} \tag{9}$$

The last quantity to be determined, related to the LTNE assumption eq.(1) and eq.(2), is the interfacial area density or particle surface area per unit volume. In the case of spherical particles it can be determined as [20]:

$$A_{fs} = \frac{6 \cdot (1-\varepsilon)}{d_p} \tag{10}$$

Latent Heat Section

The effective heat capacity method [21] was exploited to model the phase transition of the PCM. With this approach, the phase transition is modeled as sensible process, i.e. non-explicit phase change tracking, with the latent heat of fusion combined into the specific heat of the material. This so-called effective heat capacity was defined as piecewise linear profile as function of temperature. A sensitivity analysis has been performed to obtain the proper size of the time step which ensures that the effect of the PCM phase transition is properly considered.

A local thermal non-equilibrium assumption was also assumed for the latent heat section of the TES and the same energy conservation equations, eq.(1) and eq.(2), for the solid and the fluid phases were solved. The only difference with respect to the sensible heat section is that the effective thermal conductivity of the solid zone is equal to the thermal conductivity of the PCM. The effect of radiative heat transfer from the metallic perforated top plate and the tube bundle was accounted for by adding a source term, on the solid zone, extracted from a 1D model [22].

The solid-to-fluid heat transfer coefficient, eq.(1) and eq.(2), was derived from the following empirical correlation developed for tube bundles [23]:

$$Nu_{latent-section} = \frac{h_{fs} \cdot d_{enc}}{k_g} = 0.51 \cdot C_{row} \cdot Re_{max}^{1/2} \cdot Pr^{0.37} \cdot \left(\frac{Pr}{Pr_s} \right)^{1/4} \tag{11}$$

valid for $40 \leq Re_{denc} \leq 1'000$ and and $0.7 \leq Pr \leq 500$. The correction factor C_{row} needs to be specified in the case the tube bundle is constituted by less than 20 rows; concerning the TES prototype under investigation, the correction factor assumed was 0.95. The fluid Prandtl number Pr is evaluated at the fluid temperature while, Pr_s is the fluid Prandtl number evaluated at the solid temperature, i.e. external surfaces of the pipes. The Reynolds number, $Re_{max} = \rho \cdot V_{max} \cdot d_{tube} / \mu$, is computed considering the maximum fluid velocity occurring within the tubes bundle:

$$V_{max} = \frac{S_t \cdot V_0}{S_t - d_{enc}} \tag{12}$$

where S_t is the transverse pitch orthogonal to the airflow direction and V_0 superficial velocity that would exist assuming an empty channel and d_{enc} is the external diameter of the encapsulation.

RESULTS AND DISCUSSION

The reference experimental test, replicated with the CFD model developed, was characterized by a charging of 3.25 h followed by a long discharging until reaching dead-state condition. The temperature of the HTF during the test was up to 595°C during charging and ambient temperature, about 20-22°C, during discharging. On average, the HTF mass flow rate during charging and during discharging was about 0.013 kg/s. Figure 2 and Fig. 3 show the comparison between CFD simulation results (solid lines) and the reference experimental data (markers). The temperature evolution measured by the TCs located in the latent heat region, along with those on the internal surface of the containing tank, are reported in Figure 2; while, the temperature measured by all the TCs positioned into the packed bed, sensible heat region, are depicted in Figure 3. Figure 4 shows the temperature contours in the TES prototype at different times during charging and discharging. A fairly good agreement between simulation results and experimental data was obtained for all the TCs but, analyzing the results obtained, it is evident that the accuracy of the model developed, in predicting the thermo-fluid dynamics behavior of the TES prototype, is satisfactorily concerning the charge phase. Nevertheless, it needs to be improved for the discharging wherein the numerical model tends to underestimate the combined TES performance. This can be improved by implementing a more accurate approach for the modeling of radiation effects which, in the upper region of the TES, play an important role. The channeling effect can be clearly observed comparing the measurement of the TCs located along the packed bed axis, T8 and T10 especially, with those radially positioned with respect to the axis (T9 and T11). Considering the TCs at the same axial position, those radially positioned showed higher temperature even up to 30°C difference. From a graphical standpoint, the channeling effect is also well visible in the temperature contour plots of Figure 4. Looking at the experimental results, another interesting aspect is related to the latent heat section of the TES: adding a small amount of PCM at the top of the packed bed allowed to observe a stabilization of the temperature (T1) of the HTF at the PCM melting temperature. This effect was also well predicted by the numerical model.

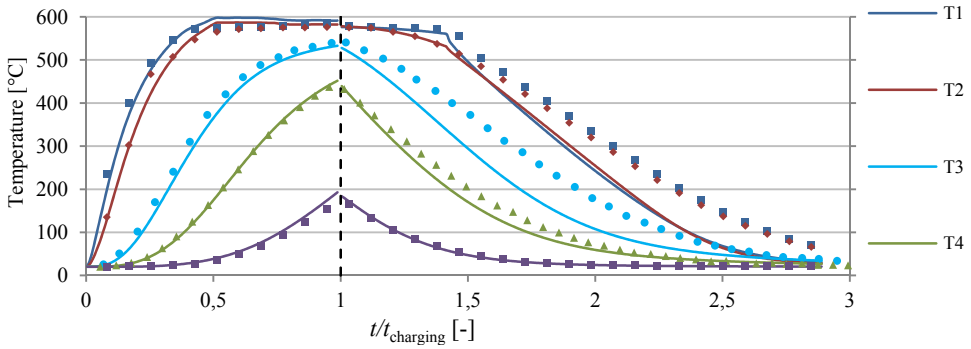

FIGURE 2. PCM and tank wall temperatures: CFD simulation results (solid lines) and experimental data (markers).

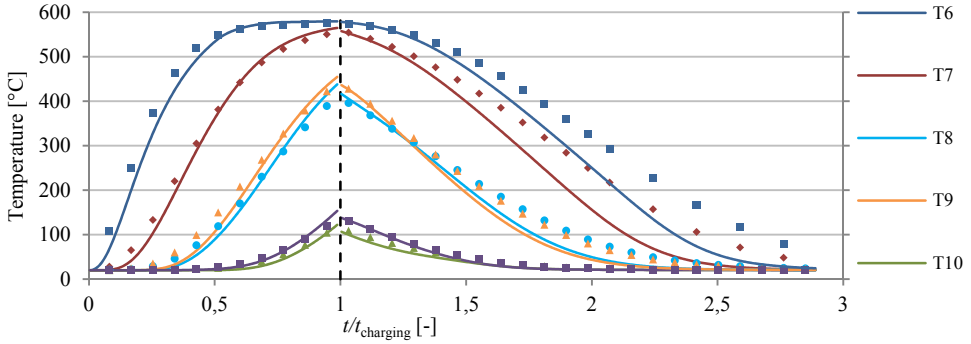

FIGURE 3. Packed bed temperatures: CFD simulation results (solid lines) and experimental data (markers).

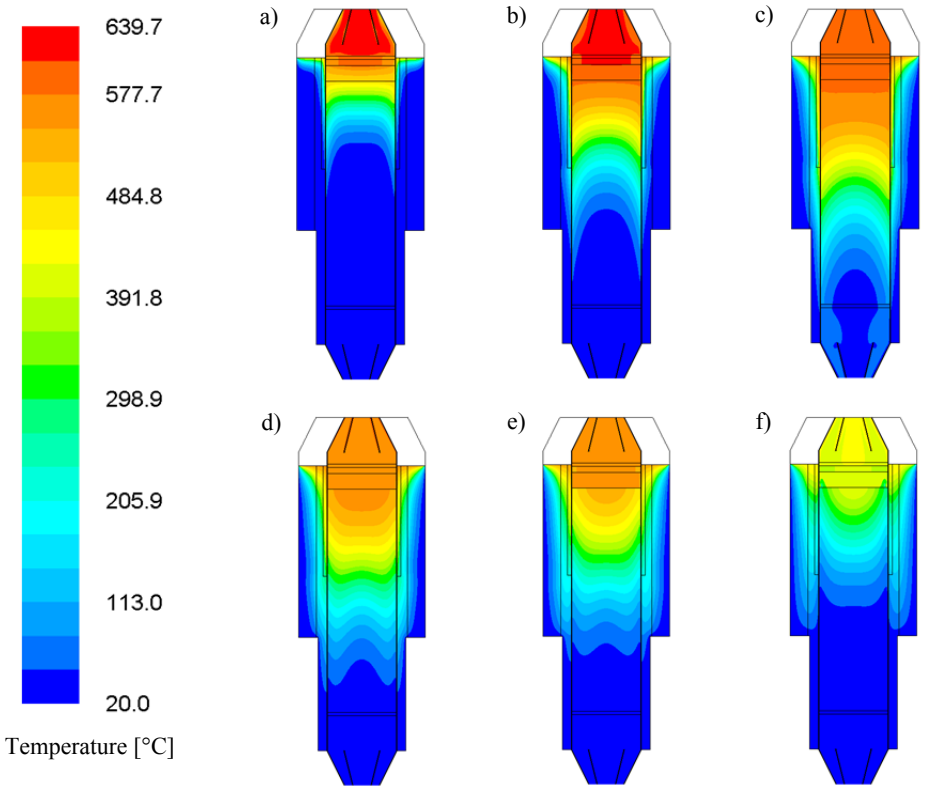

FIGURE 4. Temperature contours during charging: a) 1.15 h; b) 2.25 h; c) 3.25 h and discharging: d) 0.55 h; e) 1.15 h; f) 2.25 h.

CONCLUSIONS

A 2D CFD model of a lab-scale combined sensible/latent heat TES was satisfactorily validated with experimental data. The 2D computational domain considered allowed to include also the radial variation of the void-fraction into the packed bed. The overall agreement between simulation results and experimental data is fairly good. However, further effort is still required to increase the accuracy of discharge phase results.

On the basis of the experimental data, the addition of a small amount of PCM on top of the packed bed seems to be a promising solution for stabilizing the HTF outflow temperature during discharging. Furthermore, due to the small tank-to-particle diameter ratio, the thermo-fluid dynamics behavior of the combined TES prototype was significantly affected by the radial variation of the void-fraction.

ACKNOWLEDGMENTS

This work has been developed in the framework of the SolAir-3 Project ("SI/500926") financed by the Swiss Federal Office of Energy (SFOE - OFEN - BFE). The support to the development of this work by the Swiss Competence Center for Energy Research (SCCER) on Heat and Electricity Storage is also gratefully acknowledged.

REFERENCES

1. REN21, "Renewables 2016 - Global Status Report", 2016.
2. G. Zanganeh, R. Khanna, C. Walser, A. Pedretti, A. Haselbacher, A. Steinfeld, "Experimental and numerical investigation of combined sensible-latent heat for thermal energy storage at 575 °C and above", Solar Energy **114**, 77-90 (2015).
3. H.K. Versteeg, W. Malalasekera, "An Introduction to Computational Fluid Dynamics: The Finite Volume Method Approach", Harlow, England: Longman Scientific and Technical, (1995).
4. T.H. Shih, W.W. Liou, A. Shabbir, Z. Yang, J. Zhu, "A new k-epsilon eddy viscosity model for high Reynolds number turbulent flows: Model development and validation," Computers and Fluids, **24**(3), 227-238 (1994).
5. J. Tu, G.H. Yeoh, C. Liu, "Computational Fluid Dynamics – A practical approach", (2008).
6. D.A. Nield and A. Bejan, *Convection in Porous Media*, (Springer, 2006).
7. ANSYS, "FLUENT - Theory guide" (2012).
8. F.P. Incropera, D. Dewitt, T. Bergman, A. Lavine, "Fundamentals of heat and mass transfer", (2007).
9. A.E. Scheidegger, "The phisics of fluid flow through porous media. Third edition", (1974).
10. D.E. Beasley, J.A. Clark, "Transient response of a packed for thermal energy storage", J. Heat Mars Transfer. **21**(9), 1659-1669 (1984).
11. Verein Deutscher Ingenieure, "VDI Heat Atlas - Second edition", (2010).
12. A.M. Ribeiro, P. Neto, C. Pinho, "Mean porosity and pressure drop measurements in packed beds of monosized spheres: Side wall effect", Int. Review of Chemical Engineering **2**(1), 40-46, (2010).
13. M.L. Hunt, C.L. Tien, "Non-darcian flow, heat and mass transfer in catalytic packed-bed reactors." Chem. Eng. Sci. **45**(1), 55-63, (1990).
14. D.B. Ingham, I. Pop, "Transport Phenomena in Porous Media", (1998).
15. D. Vortmeyer, J. Schuster, "Evaluation of steady flow profiles in rectangular and circular packed beds by a variational method" Chem. Eng. Sci.**38**, 1691-1699, (1983).
16. S. Yagi, D. Kunii, "Studies on effective thermal conductivities in packed beds", A.I.Ch.E. J. **3(**3), 373-381, (1957).
17. D. Kunii, J.M. Smith, "Heat transfer characteristics of porous rocks", A.I.Ch.E. Journal, **6(**1), 71-78, (1960).
18. G. Zanganeh, A. Pedretti, S. Zavattoni, M. Barbato, A. Steinfeld, "Packed-bed thermal storage for concentrated solar power – pilot-scale demonstration and industrial-scale design", Sol. Energy **86**(10), 3084-3098, (2012)
19. A.S. Gupta, G. Thodos, "Direct analogy between mass and heat transfer to beds of spheres", AIChE J. **9**(6), 751–754, (1963).
20. N. Wakao, S. Kaguei, "Heat and mass transfer in packed beds", (1982).
21. D. Poirier, M. Salcudean, "On numerical methods used in mathematical modelling of phase change in liquid metals", ASME Journal of Heat Transfer **110,** 562-70, (1988).
22. L. Geissbühler, M. Kolman, G. Zanganeh, A. Haselbacher, A. Steinfeld, "Analysis of industrial-scale high-temperature combined sensible/latent thermal energy storage", Applied Thermal Eng. **101**, 657-668, (2016).
23. A. Zukauskas, "Heat Transfer from Tubes in Cross Flow", Advances in Heat Transfer **8,** (1972).